JET–P(98)83

P Smeulders et al

Characteristics of a new Class of Transport related MHD Modes in JET H-mode Plasmas

JET–P(98)83

Characteristics of a new Class of Transport related MHD Modes in JET H-mode Plasmas

P Smeulders, G D Conway, B Alper, B Balet, D V Bartlett, D Borba, N Deliyanakis, T C Hender[1], O J Kwon[1,2].

JET Joint Undertaking, Abingdon, Oxfordshire, OX14 3EA,
[1]EURATOM/UKAEA Fusion Association, Culham Science Centre, Abingdon, OX14 3DB, UK.
[2]Permanent address: Dept of Physics, University of Taegu, Republic of Korea.

Preprint of a Paper to be submitted for publication in
Plasma Physics and Controlled Fusion

February 1999

ABSTRACT

A new type of MHD mode , provisionally termed the Wash Board (WB) mode, has been observed during H-mode plasmas in JET. It occurs in all types of H-mode discharges, but is not seen during L-mode even at high values of β. The WB mode appears to be linked with saturation in the plasma confinement and central plasma temperatures.

These modes have high m and n numbers and are localised in the outer part of the plasma, typically from the q=2 surface to the plasma edge. They rotate with the electron diamagnetic frequency and have a strong ballooning character.

There is a good correlation between increasing plasma pressure and the growth of both the spectral extent and amplitude of the WB modes. Changes in the electron temperature profile also correlate well with changes in the amplitude of these modes. They are therefore regarded as a possible candidate to explain the power degradation of the empirically established H-mode scaling laws.

1. INTRODUCTION

MHD activity in general has been observed to limit performance at various stages in JET discharges [1,2,3] and in other fusion devices [4,5,6,7]. The modes associated with the performance degradation are usually localised in time, for example Outer Modes, Sawteeth and ELMs [1]. During the evolution of the H-mode phase in JET however, there is a diffuse background in the spectra of the signals from magnetic pick-up coils which is observed to increase as β increases.

This background can contain two types of modes: one which rotates in the electron diamagnetic direction with mode frequencies between 10 kHz and ~100 kHz and, if β is high enough, a second type rotating in the opposite direction at higher frequencies (100 kHz to 200 kHz) but below the TAE frequency [17]. The “electron diamagnetic” modes start shortly after the L-H transition at β_N ~1, where β_N is the normalised β, $\beta_N = \frac{\beta(\%)}{I(MA)/B(T)a(m)}$. Occasionally, modes are observed [8] at even higher frequency. These are also associated with a saturation or decline in confinement. This paper investigates the “electron diamagnetic” modes. The “ion-diamagnetic” modes are discussed in [17].

This new type of mode has been named the WB or “Wash Board” mode because of its characteristic appearance on time-frequency contour plots, which resembles the periodic ridges on an old-fashioned washboard. This can be seen in the lower part of fig.1 and more clearly in fig.2, both of which show the spectrum of a magnetic pick-up coil at the low field side (37° above the mid plane) as a function of time. These figures will be discussed in detail in section 2.

These modes have been seen before [1] in JET with a system of comb filters, but at that time no other diagnostic had a suitable time resolution to analyse their structure in more detail.

The WB modes appear in the frequency spectra as a set of stripes at discrete frequencies which evolve slowly in time. The amplitude of the modes is not constant. They pulsate on a time scale of the order of ~250 μs or less, as can be seen in fig.2. This has an effective time resolution (due to the time span of the Fourier transforms) of 250 μs. The WB modes rotate in the electron diamagnetic direction, which is against the core plasma toroidal rotation, induced by the neutral beam injection. The mode frequency is of the same order as the electron diamagnetic frequency at the plasma edge. However at radii where the modes are located their frequency is higher than the electron diamagnetic frequency, especially when the superimposed toroidal plasma rotation is taken into account. This is discussed further below. There can be many WB modes spread over a frequency range of 10 kHz to several 100 kHz.

The remainder of this paper is organised as follows. In section 2 the types of discharge and the conditions in which these modes occur are described. In section 3 the topology of the WB modes in the radial, poloidal and toroidal directions is presented. Further properties, such as their ballooning character and phase as a function of radius, are discussed in section 4.In section 5, several possible candidates to explain the WB modes, including resistive ballooning modes, are considered. Finally, section 6 demonstrates the importance of the WB modes for plasma transport in H-mode discharges.

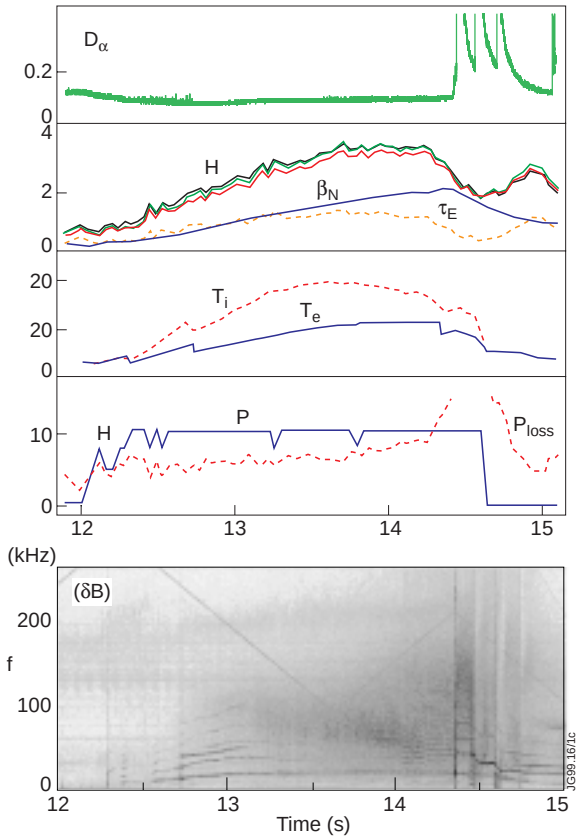

Fig1. Time traces of various parameters in the Hot-Ion H-mode phase of Tritium discharge #42840, with I_p = 3.9 MA, B_T = 3.4 T. From top to bottom: (i) the $D\alpha$ trace, (ii) the nearly identical Goldston, JETDIII-D and ITER89-P H-multipliers together with the plasma normalised pressure β_N and the energy confinement time τ_E, (iii) the central ion T_i and electron T_e temperatures, (iv) the NBI input power P and the loss power P_{loss}. The time evolution of the spectrum of the fluctuating signal from a magnetic pick-up coil at the low field side 37° up from the mid plane is shown at the bottom. The amplitude scales are logarithmic. Around 53 s the pattern of modes which we refer to as "washboard" modes starts to grow between 0 and 150 kHz. A sawtooth occurs at 54.34 followed by post-cursor modes, Outer Modes and ELM's, which leads to the termination of the Hot-Ion H-mode phase. The n=1 mode and its harmonics present in the early stages of the heating phase die out after 53 s. There is also a frequency sweep visible between 100 and 300 kHz by the TAE excitation coils.

2. OPERATION SPACE

The WB modes occur only during the H-mode phase of JET discharges. Moreover, they occur in ***all*** H-mode discharges: ELM-free Hot-Ion H-modes, ELMy H-modes, Optimised Shear, and

ICRH heated discharges. They do not occur in the L-mode phase even at relative high plasma β, e.g. the Optimised Shear discharges with β_N of 1.8. They have been characterised in all the major types of JET discharge.

ELM-free Hot-Ion H-modes

The WB modes start to appear soon after the L to H transition as seen from their negative m and n numbers (the assumed convention is that positive/negative mode numbers rotate in the ion/ electron diamagnetic direction, respectively). Their rapid growth is well correlated with the saturation of the H-factor and the central ion temperature. There is a simultaneous reduction in the rate of rise of the central electron temperature.

The lower part of fig.1 shows the growth of the WB modes as a function of time as measured by a magnetic pick-up coil. Also visible in the figure is a variety of other forms of MHD activity including n=1 activity (at ~ 15-20 kHz) which is present in particular at the beginning of the good confinement phase. The m=1, n=1 activity and its higher harmonics diminish after t = 53 s. This is discussed in a separate paper on the Tritium discharges [9]. The near identical evolution's of the H-factors for the Goldston, JETDIII-D and ITER89P scalings are also shown. It is clear that the H-factor saturates when the WB modes become well established in their frequency extent and amplitude. The saturation of the H-factor and the decline in the energy confinement time τ_E occur as the effective input or loss power P_{LOSS} increases from 6 to 9 MW (no compensation has been made for the fast particles present). Apart from the decline in the confinement time, the power degradation also manifests itself as a saturation of the central ion temperature and a reduction in the rate of rise of the central electron temperature (solid curve). It also can be seen that growth of these high frequency modes and the growth in β_N go hand in hand, as shown in the second figure from the top.

The sudden change in the spectrum of the WB modes between 20 kHz and 50 kHz, at time t_2=54.0 s is clearly visible in fig.2. It leads to a clear reduction in the rate of rise of the whole electron temperature radial profile, as can be seen in fig.3. Even more revealing is that, following the sawtooth crash, the WB modes stop and the temperature at the edge rises again.

There is another important detail just visible in the spectra of fig.2, which has a time resolution of 250 μs. The amplitude of the WB modes is not constant in time, and the frequency of the modes is not fixed. The WB modes occur in bursts of ≤250 μs duration.

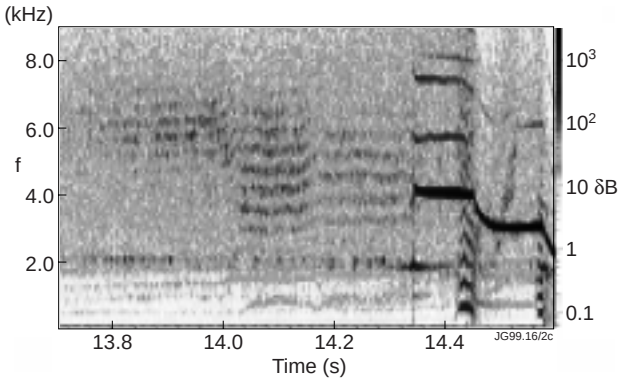

Fig.2. Fourier spectra of the WB modes of discharge #42480. Note the sharp increase in WB mode activity around t=54.05 s in the lower frequency range. A sawtooth occurs at 54.34 s with a precursor at 20 kHz, followed by neo-classical type (4,3), (6,4), (7,5) modes at 40, 57, 74 kHz. ELMs and Outer Modes occur around 54.44 and 54.57 s.

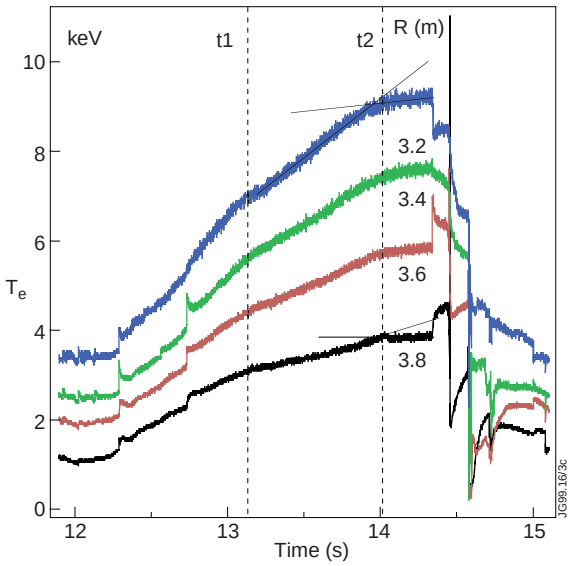

Fig.3. The electron temperature at various radial positions for discharge #42840. The plasma centre is at R = 3.05 m. The change in the rate of rise at time t_2 due to the change in WB mode activity is clearly visible on all traces (2.32 and 1.15 keV/s at R=3.2 and 3.8 m respectively). A smaller but similar effect is apparent at t_1 when there is also a notable increase in WB mode activity (fig.1).

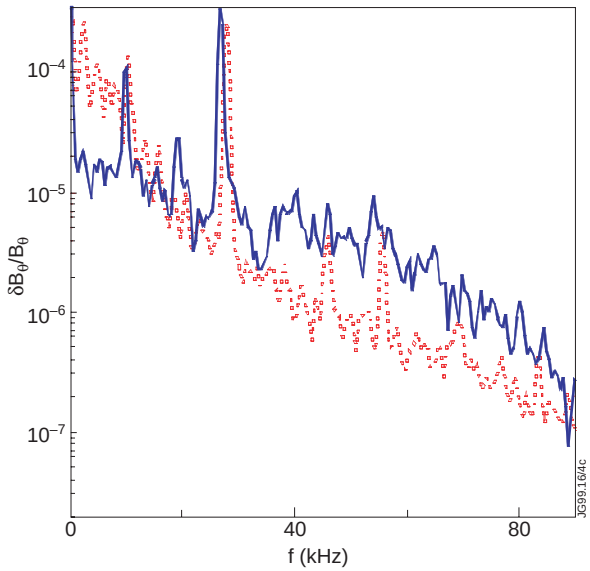

Fig. 4. Fourier spectra of signals from a magnetic pick-up coil before (—) and after(—) an ELM in the ELMy H-mode discharge #42756. There are discrete modes rotating in the ion-diamagnetic direction at around 10 kHz and 28 kHz, which are coupled (1,1) and (3,1) modes, and a (4,3) mode. At 44kHz and 56 kHz are even higher(m,n) modes: ~(11,5),(12,7). The rest of the spectra are made up of WB modes, which clearly diminish strongly after the ELM. Between 30 kHz and 90 kHz the spectra contain a near-continuum of around 20 WB modes.

ELMy H-modes

The ELMy H-mode discharges which have been analysed are characterised by a series of large ELMs immediately followed by a series of smaller ELMs and short intermittent ELM-free periods of around 100 msec [2]. WB modes are present in at least the outer part of the plasma during all of this time. Central MHD activity (sawteeth and fishbones) has little effect on the WB modes.

ELMs have a dramatic influence on the WB mode amplitude. This is shown in fig.4, which shows the spectrum before and after an ELM . The many overlapping WB modes, resulting in a "noisy" spectrum, drop about a factor of 5 in amplitude at each ELM. Edge MHD activity is clearly important to the development of the WB modes, since only edge modes (ELMs and Outer Modes) affect the WB modes both in amplitude and rotation. We therefore conclude that the driving force of the WB modes must be located close to the plasma edge.

Optimised Shear H-modes.

During the L-mode phase of Optimised Shear discharges no WB modes are observed, although there are other modes such as chirping modes [3] which rotate in the ion-diamagnetic direction and are located near the transport barrier. However, shortly after the L to H transition, modes rotating in the electron diamagnetic direction appear with a similar structure to those in the ELM-free and ELMy discharges. Because the density profile is still peaked even in the H-mode

phase of the discharge, density fluctuations can be measured by the O-mode reflectometer up to the plasma centre. Generally there seem to be fewer WB modes in the Optimised Shear discharges. This is consistent with the trend in fig1, which shows that the number of WB modes increases approximately in proportion with β. The β in the Optimised Shear discharges is generally 25% lower than in the Hot-Ion H-modes.

Neutral Beam heated versus Ion-Cyclotron heated plasmas

No difference in the characteristics of the WB modes has been found when comparing discharges heated by NBI only with those which have substantial ICRH heating. These latter discharges have a large non-thermal ion population (30% of the total plasma stored energy), but this does not seem to have an effect on the WB modes. This indicates that the WB modes are related to the thermal population of the plasma (N.B. fast particle modes always rotate with ω_{*I}).

3. LOCALISATION

WB modes are visible not only as magnetic fluctuations but also as fluctuations of the electron density and, weakly, of the electron temperature. Therefore the radial position of the WB modes can be found by determining the radial location of the density and temperature fluctuations. The WB modes are strongly modulated by ELMs (as shown in fig.4) and also by Outer Modes (Outer Modes are external kink modes localised near the plasma edge [1]). This suggests that their origin must lie close to the plasma edge. However, in Optimised Shear discharges, which have a sufficiently peaked density profile that the O-mode reflectometer can measure to almost the plasma centre, it is found that the density fluctuations associated with the WB modes extend from the edge into the transport barrier and occasionally beyond (fig.5).

The reflectometer is well suited to measuring small scale density fluctuations. These can be translated into radial displacements of order of 1 mm or less, allowing reliable information about the localisation of the WB modes to be obtained. There are 4 clear WB modes at 37, 42, 49 and 54 kHz present in the reflectometer data for the Optimised Shear discharge shown in fig.5. Also present at 29 kHz is a (8,3) mode with $\delta B\theta/B\theta \sim 4.10^{-4}$, and at 60 kHz a (4,3) mode rotating in the ion-dia-

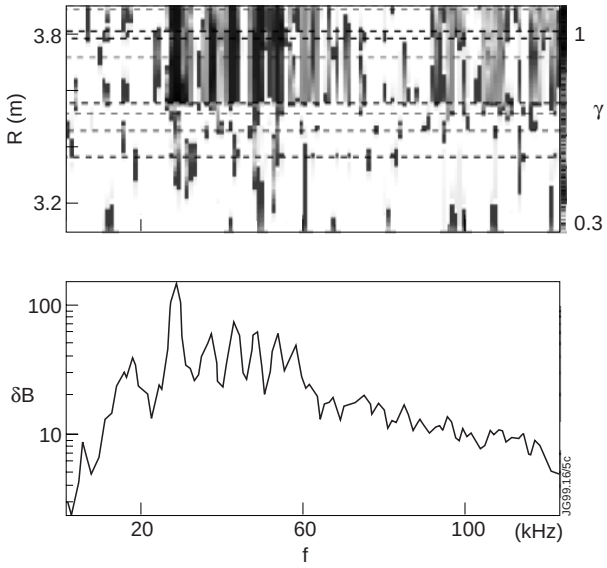

Fig.5. Spectrum of the coherence γ of the electron density fluctuations with the grey scale of γ on the right as function of major radius R in m over t = 46.859-46.875 s as measured with the JET reflectometer system in an Optimised Shear discharge 41629 with a peaked density radial profile. The foot of the transport barrier of the discharge is at 3.55 m. The bottom figure is the power spectrum of the reference signal dB against which the coherence is calculated, a magnetic pick-up coil at the same octant but separated by θ=40° poloidally and ϕ=-13° toroidally from the reflectometer probing beam.

magnetic drift direction. There is strong coherence over the region outside the internal transport barrier at R ≈ 3.55 m, and significant coherence ($\gamma > 0.5$) in the core for some of the modes.

Information on T_e fluctuations due to WB modes, obtained from the Electron Cyclotron Emission (ECE) heterodyne radiometer is less useful. The fluctuations are small ($\delta T_e \sim$ 10-20 eV) and are generally obscured by the thermal fluctuation level of the ECE from a 10 keV plasma, leading to large error bars in the analysis. The technique of extracting as much as possible information from these small fluctuations out of the spectra is described in the appendix 3.

Figure 6 shows the radial displacements deduced from T_e and n_e fluctuation data for the 42 kHz mode with $\delta B_\vartheta/B_\vartheta$ of ~ 10^{-5} and a (m,n) mode structure of (-14±2,-7±1). The displacements are of the order of 1 mm and for this particular mode extend to the plasma core. These results show that the WB modes start at the plasma edge with low levels of displacement (~0.1 mm) and increase to ~1 mm at the transport barrier (R~3.55 m) and beyond.

In Hot-Ion H-modes with a high Tritium concentration and moderate NBI power, the general level of MHD activity is strongly reduced and the WB modes can be observed alone over prolonged periods, up to several hundred ms. Figure7 shows the displacements obtained from the reflectometer and ECE data, in the same way as fig.6, for a 47 kHz mode. The flat density profile limits the O-mode reflectometer to measurements close to the plasma edge, but the ECE measurements suggest that this mode, at this particular time, extends almost to the plasma centre (R=3.05 m). The error bars are again derived from the statistics of the offset Gaussian fit to the temperature fluctuation spectra. Due to the large error bars, only an approximate indication of the displacements can be obtained for this discharge.

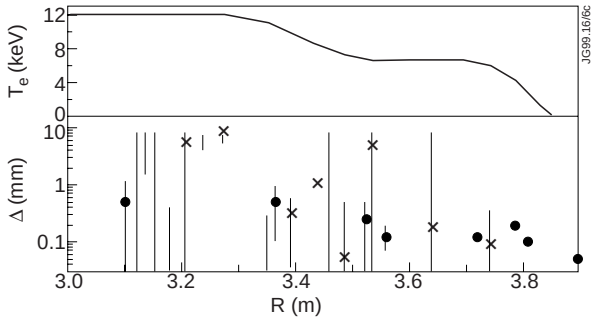

Fig.6. T_e and n_e fluctuations due to the WB mode translated into displacements by use of the measured temperature profile and the method which is explained in Appendix 1. The top figure shows a functional fit to the ECE T_e profile(solid line). The lower part of the figure shows the displacements deduced from density fluctuations (ò) and temperature fluctuations (X). The error bars are obtained from the least squares fit of an offset Gaussian to the MHD activity spectrum around 42 kHz as shown in fig.5. The error bars for the T_e displacements can be very large, due to noise in the ECE data.

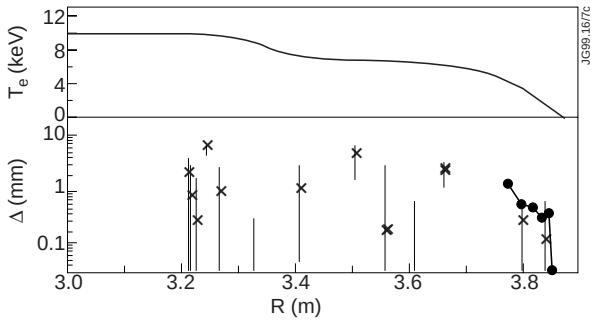

Fig.7. Displacements in a hot-ion H-mode discharge (#42840) for t = 54.049-54.065 s. The density fluctuations (ò) at 47 kHz with $\delta B_\theta/B_\theta$ ~1.5 10^{-5} can only be measured in the outer part of the plasma (R>3.7 m). The temperature fluctuations indicate that the displacements (X) in the plasma core are ~1-3 mm (±2 mm) whereas in the outer part of the plasma ~0.5-1 mm displacements are deduced from both density and temperature fluctuations.

The displacements due to the WB modes vary substantially with time, and from mode to mode. The data in fig.6 is an example of activity that has a displacement that extends to the plasma centre, but many others do not reach the plasma centre. The displacement at the plasma edge due to the WB modes can have a significant temporal variation. This is illustrated in fig. 8 for the 47 kHz mode of discharge #42840.

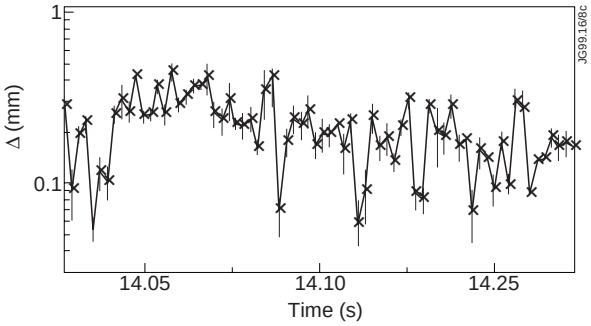

Fig.8. Displacement from n_e fluctuations, averaged over R=3.75 to 3.85 m as function of time for discharge #42840. The time resolution is limited to 4 ms by the number of points required for the coherence analysis

4. OTHER PROPERTIES

Figure 9 shows how the ballooning character of the WB modes changes with plasma β. Spectra of the signals from two magnetic pick-up coils, located at the high and low B field sides, are taken at two times with different values of β. At β_N values below unity the spectra do not exhibit any ballooning character, but at β_N of 1.2 a ballooning effect (the ratio of the amplitude on the low and high field coils) of ~3 is observed. The asymmetry grows with β to reach a factor of ~10 at β_N of 1.7 and above. The contribution of the Shafranov shift to this asymmetry can be calculated from the equilibria to be no more than a factor of 2. It can also be seen from the figure that at frequencies above ~80 kHz the ballooning effect is less evident. This seems to be linked to the ion diamagnetic modes which for f > 80 kHz overlap the frequency region occupied by the electron diamagnetic modes. These ion diamagnetic modes do not show a strong ballooning effect [17].

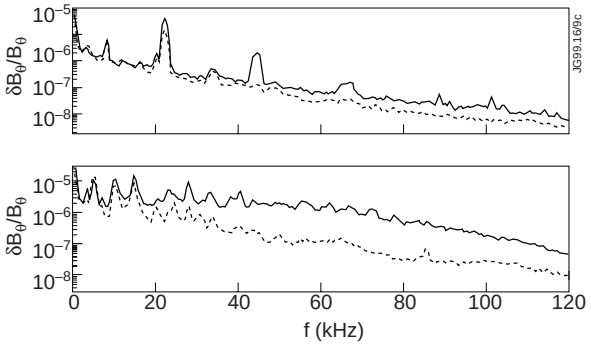

*Fig.9. Spectra of the $\delta B\theta/B\theta$ signals from magnetic pick-up coils in the Hot-Ion H-mode discharge #42676 at two different times (**a** :t = 52.43 s, **b**: t = 52.98 s) for which β_N is significantly different (0.9 and 2.2, respectively). The solid/dashed lines correspond to the coil at a poloidal position of θ = 37° (low field side) and at θ = 166° (high field side). The influence of β_N on the ballooning character of the MHD activity can be readily seen. Note that at low β the WB modes are weak compared to low n modes. At the higher β value the WB modes show up as individual modes between 40 and 80 kHz.*

The edge displacements of the various WB modes are similar in size. This can be seen in fig. 10 which shows the coherence and phase of reflectometer signals, with respect to a magnetic pick-up coil, as a function of major radius. It is apparent that the coherence of the density fluctuations in the outer plasma is close to unity for most of the WB modes. Almost all of these modes are analysed to have displacements of around 1. ±0.5 mm at R=3.8 m, but the penetration into the interior of the plasma varies from mode to mode.

Also it can be seen in fig.10 that the phase of the fluctuations, with respect to a magnetic pick-up coil in the same octant, varies from -π to π over the frequency range 24 kHz to 76 kHz. This phase variation occurs because the magnetic pick-up coil is poloidally displaced from the reflectometer measurement and is consistent with the mode numbers varying from (-7,-3) at 24 kHz to (-17,-8) at 48 kHz (see fig.11 below). At 76 kHz the spectrum of the magnetic pick-up coil is no longer determined by WB modes alone. Rather, it contains a mixture of other modes (which dominate the spectrum above 100 kHz) which are rotating in the ion-diamagnetic drift direction. It is believed that the 76 kHz mode has a poloidal and toroidal structure which is principally around m = -25, n = -12; this is illustrated in fig.11. The correction for the spatial separation of the magnetic pick-up coil and the location of the reflectometer shows that the phase of the density fluctuations is in anti-phase with the poloidal magnetic field fluctuations. Also it can readily be seen from fig. 10 that there is no phase change over radius for the WB modes

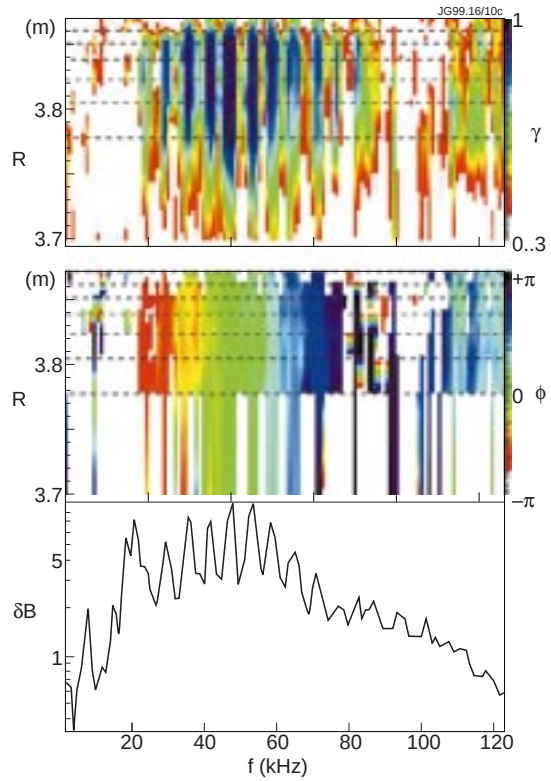

Fig.10. Coherence, γ, and phase spectra, Φ, as functions of major radius R for the discharge #42840 at t = 54.049-54.065 s. The colour scale for γ and Φ is shown at the right of each plot. The signal from a magnetic pick-up coil in the same octant is used as the reference. Its power spectrum δB is shown in the lower part of the figure. In the upper plots, the dotted lines mark the positions of the reflectometer channels. The coherence and phase values are interpolated between these radii. It is clear that there is no phase inversion over radius for the various WB modes between 25 and 75 kHz.

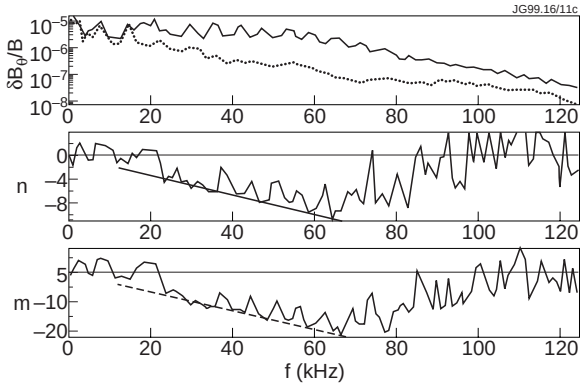

Fig. 11. Fourier spectra of signals from low (solid) and high (broken) field pick-up coils and the derived toroidal n and poloidal m number of the WB modes, for discharge #42840 for t=54.049-54.065 s. The modes have negative (m,n) numbers and stretch from 10 kHz to above 80 kHz. Their phase velocity is about 1.5 10^4 m/s.

The magnetic structure of WB modes has been analysed using combinations of toroidally and poloidally spaced magnetic pick-up coils. Typical magnetic mode numbers are in the range of m = -3 to -30 and n = -1 to -15. The toroidal set allows for a resolution of n=±60 (corresponding to a 2π phase jump) and by using the θ^* effect as explained in appendix 2, a similar resolution in the m-number can be obtained. The resulting m and n numbers are shown in fig. 11 for the same discharge and time span as fig.10.

Several general characteristics of the WB modes emerge from the above analysis. The WB modes are small scale fluctuations with a scale length (radial displacement) of the order of 1 mm. There are many of these modes over the frequency range of the measurements and they have a varying radial extent, with some reaching almost to the plasma core at certain times. The rotation of the WB modes is in the direction of the electron diamagnetic drift velocity. The phase velocity of the modes $v_{phase}= \omega/k$ is around 1.5 10^4 m/s with $k = \sqrt{\frac{m^2}{r^2} + \frac{n^2}{R^2}} \approx \frac{m}{r}$. This is close to the electron diamagnetic drift velocity, v_{de} , at the plasma edge of 10^4 m/s , but larger than v_{de} at the plasma interior where $v_{de}\sim 5.10^3 \times r$ m/s with r the plasma minor radius (typically ~0.7-0.8 m). Except for the plasma edge, the true phase velocity is probably even higher because the toroidal plasma rotation induced by the NBI is superimposed on this and reduces the apparent mode frequency.

The WB modes fluctuate in strength. The time scale of this fluctuation cannot be accurately determined from the present data because of the sampling rate of the data acquisition (≥2 μs) and the minimum number of samples of 256 required in the analysis. However, the time scale is certainly well below 1 ms and may be of the order of 100 μs.

5. INTERPRETATION.

There are several clues to the nature of these modes in the data discussed above. The fact that they rotate in the electron diamagnetic direction tends to indicate that they are resistive type modes. However, there are several arguments which demonstrate that they are not tearing modes (i.e. those which form magnetic islands).

The measured magnetic fluctuation amplitude at the resonant surface can be calculated to be approximately $\delta B_\theta/B\theta \sim 10^{-3}$-$10^{-4}$ following the r^{-m} dependence [10]. Using the technique described in [10] we have,

$$w = 4\sqrt{\frac{rq\widehat{B}_r}{mq'B_\vartheta}} \approx 4r\sqrt{\frac{\delta B_\vartheta}{B_\vartheta}\frac{1}{ms}} \qquad (1)$$

which yields "island" widths of w~ 5-10 mm, when m, the poloidal mode number, is taken to be ~17, and the shear, s,(s = rq′/q) to be ~1-2. This calculated island size is roughly an order of magnitude larger than the displacement inferred from the ECE and reflectometer data, indicating that these are not magnetic islands. Further, the reflectometer cross-correlation results in

fig.10, which show that none of the WB modes experiences a phase change across the observable radius range, are inconsistent with an explanation in terms of magnetic islands, which would exhibit a π phase change. The final clue to the nature of the WB modes is that they have a strong ballooning character which increases with β.

These observed characteristics of the washboard modes are consistent with many of the features of resistive ballooning modes (RBMs). Obviously the observed ballooning character is consistent with these type of modes. Furthermore RBMs rotate in the electron diamagnetic direction [11] and have twisting (not a tearing) parity [12]. However, as is well known collisional resistive ballooning modes have a relatively slow growth rate and are damped by sound waves (which 'connect' the good and bad curvature regions) [13]. As a result collisional resistive ballooning modes are unstable only very near the plasma edge (where T_e is low, resistivity is high and sound wave propagation is slow) [14]. This has been checked by calculating the RBM stability for pulse #42840 at radii where the WB modes are observed. Figure 12 shows the growth rate of the RBM at R=3.7m as a function of the magnetic Reynolds number ($S=\tau_R/\tau_A$). It can be seen that the experimental value for n^2/S is well below the RBM critical value of $7\ 10^{-4}$.

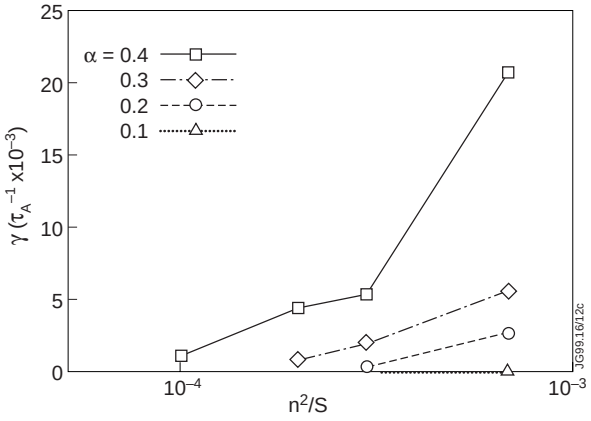

Fig. 12. Calculated value of RBM growth rate (in poloidal Alfven units) versus n^2/S for several values of normalised pressure gradient ($\alpha=-(2\mu_0 r^2/RB_\theta^2)dP/dR$). At R=3.7m the measured value is $\alpha=0.11$ and for n=10 (typical for a WB mode), $n^2/S=1.6x10^{-7}$. In the RBM calculation the value of the measured sound speed is used.

In fact, the low collisionality at the radii where WB modes are observed means that collisional resistive MHD is not really applicable. Several authors have proposed theories which give a resistive ballooning type mode but with modified drive terms. Itoh et al have proposed a transport theory [15] in which the anomalous dissipation from mode turbulence provides a drive for RBM-like modes (which themselves are the source of the turbulence, so that resistivity plays no role). Alternatively Kleva and Guzdar have shown that electron inertia can destabilise RBM-type modes in the collisionless limit [16]. It thus remains possible that the observed WB modes are RBM-type modes with the drive provided by some other type of dissipation.

6. TRANSPORT

The WB modes provide a possible explanation for the observed anomalous transport in H-modes. They have several characteristics typical of modes causing turbulent transport, being numerous, small radial displacement, short lived, present over a large part of the plasma cross-

section and having an amplitude which increases with plasma pressure. They could therefore lead to a turbulent-like, diffusive transport with a diffusivity given by $\chi_{eff} = N\frac{\Delta^2}{\tau}$, N(R) being the number of modes involved, Δ the average displacement of the assembly of modes and τ the typical growth/decay time of the modes. Taking N~20 in the outer plasma, Δ~2 mm, τ~200μs yields χ_{eff} =0.4 m^2/s, which is the correct order of magnitude.

The study of the correlation of WB mode activity with transport is not an easy task, since the plasma transport and confinement depend on a large set of parameters. The problem can be addressed in two different ways: (a) comparing global parameters related to transport and confinement with a set of parameters characterising the WB mode activity or (b) comparing the local transport with the changes in the local WB mode activity. The first approach is summarised in fig.1. The second approach is complicated by the fact that various types of MHD fluctuations have been found to influence the plasma confinement. Among the most common are Sawtooth oscillations, Edge Localised Modes (ELMs) and Outer Modes (external kinks). Trying to isolate the effect of all the different types MHD oscillations on the plasma confinement is impossible in the presence of a large variety of MHD phenomena in the same discharge. Hence, a set of discharges has been selected which is characterised by a long quiescent period free from any MHD activity except WB modes. In these discharges the level of WB activity is compared with the evolution of ion and electron temperatures.

The discharges with high concentrations of Tritium and moderate NBI heating which were produced during the JET alpha heating experiments [9] are characterised by periods with little or no MHD activity other than WB modes. Additionally, in two of these discharges (#42847 and #42840) there is a sharp transition in the level of WB mode activity (as was shown in fig.2). By studying the evolution of the electron temperature during this sharp transition we can investigate the influence of this MHD activity on the plasma confinement. In discharge #42840 the transition occurs at t=54.05 s (fig.2). In fig. 3, the changes in the electron temperature at various plasma positions during the increase (at $t = t_2$) in WB mode activity are shown. Before the transition the temperature at R=3.6 m is increasing linearly at a rate of 1.7 keV/s and after the transition the rate of rise falls to 0.3 keV/s. Also note that the start of the WB modes coincides with another change in the rate of rise of the electron temperature, at $t=t_1$.

It is difficult to prove beyond doubt that WB modes are responsible for the power degradation. However, another result also points to their importance: there is a good correlation between an increase in the electron plasma heat conductivity and an increase in WB mode activity. Figure 13 shows the χ_e (R,t) calculated by TRANSP [20] for the same discharge as fig.2. At 53 s the χ_e is low nearly everywhere, but it then increases gradually, starting from the edge. At the same

time, 53 to 54.3 s (see fig. 1) the WB modes start to grow in amplitude and in number. From 53.7 s onwards changes in WB modes are reflected in changes in χ_e, particularly around 54.0 s. The change around 54 s in the WB mode activity is associated with changes of the χ_e in the region between 3.6 - 3.8 m from 0.06 to ~0.2 m^2/s.

These results show that the WB modes have a clear influence on the plasma confinement in H-mode discharges. However, even if they do explain the power degradation in H-modes, other mechanisms must be invoked for such a degradation in L-mode in which WB modes do not occur. As discussed in [17], at higher β the high frequency modes rotating in the ion-diamagnetic direction are possibly β-induced temperature gradient (BTG) eigenmodes and are also seen to have an effect on the plasma transport. These modes are very weak in the Hot-Ion discharge discussed in this paper.

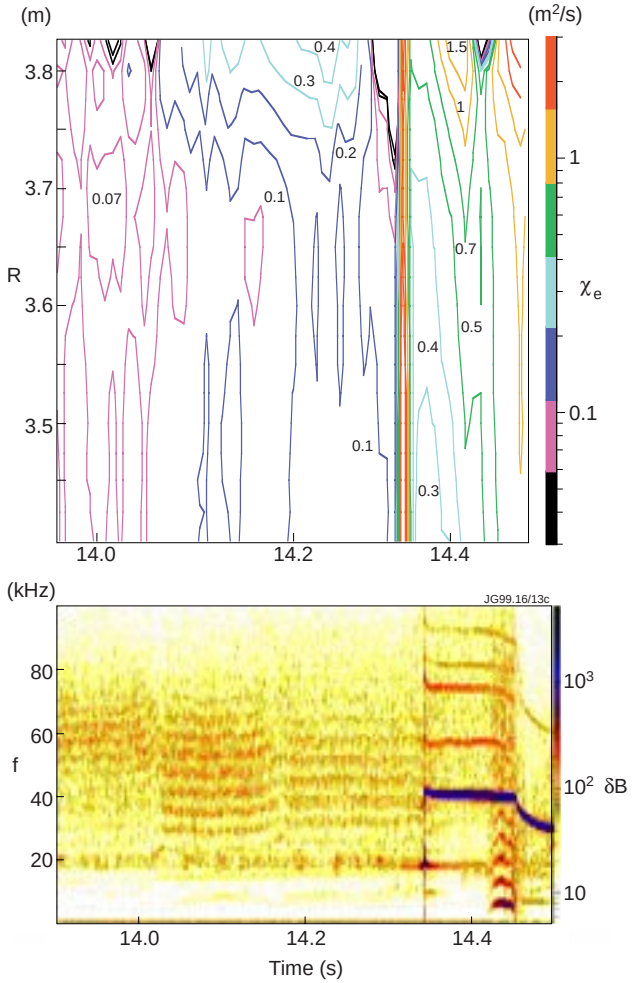

Fig.13. The electron heat conductivity $\chi_e(t,R)$ over the same period as the data of fig. 2 in the Hot-Ion H-mode #42840. The change in electron heat conductivity at 54 s is associated with the change in the WB mode spectra. This is a clear indication of the effect of the WB modes on plasma transport. The changes after 54.34 s are related to other MHD phenomena: Sawtooth, Neo-classical type of modes, Outer Modes and ELMs.

SUMMARY

The WB modes are clearly linked with the H-mode phase of JET discharges. They grow in amplitude and expand in frequency with increasing β. They have a strong ballooning character and do not appear to be of a tearing type. Typical radial displacements as deduced from density and temperature fluctuations are of the order of few millimetres. The mode amplitude varies strongly in time with a time constant of less then 250 μs. It appears most likely that the WB modes originate in the plasma edge but extend further inwards, occasionally to the plasma centre. There are many more WB modes in the outer part of the plasma than in the core. The WB modes appear to be linked to the saturation in H-mode plasma confinement and their properties are consistent with measured electron transport.

The precise nature of the WB modes still needs further theoretical investigations.

ACKNOWLEDGEMENTS.

It is a pleasure to acknowledge the invaluable contribution of Dr. Alan Edwards and of Mr. Ken Blackler, who are responsible for the new data acquisition system CATS, which forms an essential basis for this analysis.

Also the encouraging comments and valuable criticism of Dr. Paul Thomas and Dr. Jack Connor are highly appreciated. The authors of course are in debt to the whole JET Team, without them there would not have been these splendid plasmas. The UKAEA authors are jointly funded by EURATOM and the UK Department of Trade and Industry.

APPENDIX 1:

Calculation of reflection layer displacements from phase changes in O-mode reflectometer signals

A density profile change results in radial displacements of the reflection layers, which in turn lead to changes in the phases of the reflectometer signals. In O-mode reflectometry, the phase change is related only to the density profile change. In the simplest case, one can express the displacement of each reflection layer in terms of the phase change in the corresponding signal, that is ignoring changes in the density profile up to the reflection layer. A more accurate analysis of the density profile change, however, may be effected by considering the effect on each phase value of the local density profile up to the corresponding reflection layer. To allow analytical progress, one assumes that the instantaneous density profile is piece-wise linear between successive density nodes, corresponding to probed reflection layers. Then one can express the phase change $\Delta\phi_i$ in a signal reflected from a particular reflection layer i , in terms of the displacements Δ_i of each density node n_i, up to, and including, that reflection layer, as follows: $\frac{c}{2}\frac{\Delta\phi_i/2\pi}{f_i} = \Delta_0(1-F_{i1}) + \Delta_1(F_{i1}-F_{i2}) + ... + \Delta_i F_{ii}$, where the LHS represents the equivalent vacuum displacement; f_i is the channel frequency; and the coefficients F_{ij} are given in terms of the density nodes n_i by $F_{ij} = \frac{2}{3}\frac{n_i}{n_j - n_{j-1}}\left[\left(1-\frac{n_{j-1}}{n_i}\right)^{3/2} - \left(1-\frac{n_j}{n_i}\right)^{3/2}\right]$. This leads to a system of n linear algebraic equations with n+1 unknowns Δ_i; this can be solved by making an appropriate assumption, e.g. $\Delta_0 = \Delta_1$, or preferably by an optimisation procedure.

APPENDIX 2.

Determination of the toroidal and poloidal mode numbers.

The toroidal mode number n is determined with the aid of a series of magnetic pick-up coils situated at various toroidal positions. A total of 6 different coils is used, with a minimum separation of $\Delta\phi=5.6°$ and a maximum of $\Delta\phi=140.8°$. Aliasing in the toroidal mode number is therefore ± 64. The phase of each coil is obtained from a complex Fourier analysis over a variable, discrete time window of typically 256 points or 1.024 ms. Seven pairs of coil combinations are then taken, leading to seven phase differences with increasing difference in toroidal angle. Each pair with smaller difference in toroidal angle is used to prohibit further aliasing of $\pm 360°$ in the next pair up in toroidal angle difference, reducing the aliasing problem to that of the smallest angle difference. Thus seven n-numbers are obtained and then, because the biggest angle difference is most likely to have the smallest error in the phase determination (mechanical variations in toroidal and poloidal positions of the coils and vessel can lead to such errors), each n-number is weighted with its toroidal angle difference. The n-number is then the weighted average of the seven n-numbers.

The poloidal mode number m is determined from 4 pick-up coils situated at octant 3 of the JET torus. Because of the θ^* -effect [18], which makes the apparent m-number dependent on the poloidal angle, the determination of the m-number is much more complicated, in particular for those modes that are situated at the plasma boundary. However one property of an elliptical shaped divertor configuration is that the apparent m-number is close to the true m-number in the torus mid-plane at the high-field side. The apparent m-number at the low field side is much lower than the true one and the apparent m-number in the X-point locations is much higher (even ∞ at the X-point). For the divertor configuration in JET the apparent m-number, which is proportional to the derivative of θ^* with respect to θ, is practically equal to the true m-number for $\theta \approx \pi$ and the apparent m is lower at $\theta \approx 0$ for modes located in the outer plasma. The pick-up coils at the low field side are 6° apart. These are therefore used to compensate for aliasing at the high field side coils which are 50° apart. Using the θ^* effect, which implies that the m-number obtained from the latter coils must be in absolute terms higher than or equal to the number obtained from the low field side coils, the poloidal m-number is derived for each of the modes present.

APPENDIX 3.

Calculation of the fluctuation level of the ECE and reflectometer signals, and the corresponding displacements.

It is assumed that all spectra are composed of a constant background and a Gaussian function over the frequency range of interest. The background is made up of genuine noise and other broad-band fluctuations, which may be due to the instruments or the plasma. The fluctuation level for each frequency is obtained directly from the power spectrum. The reference spectrum , which is used in the coherence calculation, is used to obtain the central position and the width of the Gaussian visible in the frequency interval of interest. The spectra of each of the diagnostic channels in the relevant frequency interval is then fitted with a Gaussian of the width and central position of the reference spectrum and a background (then only 2 free parameters). These latter will vary from channel to channel. The amplitude of the fluctuation is then :

$$A = 2 * 2 * \sqrt{2\pi}\ f_0\ s \tag{2}$$

with the first factor of 2 to compensate for the Hanning window, the second one to get to the peak to peak amplitude, f_0 is the peak value of the Gaussian fit and s = 0.4247×FWHM of the Gaussian fit made to the reference spectrum. Each fit is determined by 4 parameters: f_0, s, the central position μ, and the background b. The standard deviation of each of these is then used to calculated the relative error bars of one standard deviation (67% probability interval) for the amplitude [19]

$$\Delta_A \quad = \quad \sqrt{\left(\frac{\sigma_{f_0}^2}{f_0^2} + \frac{\sigma_s^2}{s^2} + \frac{\sigma_b^2}{{f_0}^2} \right) \chi^2} \tag{3}$$

In practice only f_0 and b contribute to the error bars in amplitude if the reference signal is well chosen and therefore σ_μ and σ_s are negligible. The quality of fit χ^2 plays an important role if greater than unity and is set to unity in the above equation when smaller than one.

Except for the displacements due to density fluctuations treated in appendix 1, the calculation of the radial displacements is carried out as follows: Each fluctuation leads to a maximum and minimum level in the local radial profile of the diagnostic in question. So, except where there is a π jump in phase over radius, the radial width between maximum and minimum radial profiles gives the radial displacement due to the kink-like movement of each local fluctuation. This method will give some error at the position of the π jump in phase over radius, which has been ignored for the moment.

REFERENCES

[1] M.Nave, et al, Nuclear Fusion 37(1997)809

[2] L.D.Horton, et al, "High Fusion Power steady-state Operation in JET D-T Plasmas" , submitted to Nuclear Fusion (1998)

[3] Y.F.Baranov, et al, "Current Profile, MHD Activity and Transport Properties of Optimised Shear Plasmas in JET" , submitted to Nuclear Fusion (1998)

[4] K.M. McGuire, et al, Fusion Energy (Proc.16 Int. Conf., Montreal,1996),Vol1,IAEA, Vienna(1997)19

[5] O.Gruber, et al, Fusion Energy (Proc. 16 Int. conf., Montreal, 1996), Vol1, IAEA, Vienna(1997)359

[6] S.Ishida, et al, Fusion Energy (Proc. 16 Int. conf., Montreal, 1996), Vol1, IAEA, Vienna(1997)315

[7] R.J. La Haye, et al, Fusion Energy (Proc. 16 Int. Conf., Montreal,1996),Vol1,IAEA, Vienna(1997)747

[8] B. Alper, et al, EPS Conference, Prague, 1998

[9] P.Thomas, et al, Phys.Rev.Lett. **80**(1998)5548

[10] J.Wesson , "Tokamaks", Clarendon Press, Oxford, 1997

[11] P H Diamond et al, Nucl Fus **28**(1985)1116

[12] H R Strauss, Phys of Fluids **24**(1981)2004

[13] J W Connor et al, Plasma Phys and Contr Fus (Proc 9th Int Conf, Baltimore, 1982), Vol 3, IAEA, Vienna, (1983)403

[14] T C Hender et al, Phys of Fluids **27**(1984)1439

[15] S-I Itoh et al, Plasma Phys and Contr Fus **38**(1996) 1743

[16] R G Kleva and P N Guzdar, 'Collisionless Non-Ideal Ballooning Modes', submitted to Phys of Plasmas

[17] S.Sharapov, A.Mikhailovskii, et al, 'Interpretation of Electromagnetic Modes in the Sub TAE Frequency Range in JET', to be published (1998).

[18] H.Zohm, et al, "Mirnov coil analysis in the DIII-D tokamak using singular value decomposition method". Technical Report GA-A20886, General Atomics, San Diego,1992

[19] P.R.Bevington, "Data Reduction and Error Analysis for the Physical Sciences", McGraw-Hill Book Company, 1969

[20] Goldston, R.J., et al, J.Comput.Phys. **43**(1981)61